Molecular Dynamics of a 1,4-Polybutadiene Melt. Comparison of Experiment and Simulation

G. D. Smith*

Departments of Materials Science and Engineering and of Chemical Engineering and Fuels Engineering, 122 South Central Campus Drive, Room 304, University of Utah, Salt Lake City, Utah 84112

W. Paul

Institut für Physik, Johannes-Gutenberg Universität, 55099 Mainz, Germany

M. Monkenbusch, L. Willner, and D. Richter

Institut für Festkörperforschung, Forschungszentrum Jülich, 52425 Jülich, Germany

X. H. Qiu and M. D. Ediger

Department of Chemistry, University of Wisconsin—Madison, Madison, Wisconsin 53706

Received July 14, 1999; Revised Manuscript Received October 12, 1999

ABSTRACT: We have made detailed comparison of the local and chain dynamics of a melt of 1,4-polybutadiene (PBD) as determined from experiment and molecular dynamics simulation at 353 K. The PBD was found to have a random microstructure consisting of 40% cis, 50% trans, and 10% 1,2-vinyl units with a number-average degree of polymerization $\langle X_n \rangle = 25.4$. Local (conformational) dynamics were studied via measurements of the ^{13}C NMR spin−lattice relaxation time T_1 and the nuclear Overhauser enhancement (NOE) at a proton resonance of 300 MHz for 12 distinguishable nuclei. Chain dynamics were studied on time scales up to 22 ns via neutron spin−echo (NSE) spectroscopy with momentum transfers ranging from $q = 0.05$ to 0.30 Å^{-1}. Molecular dynamics simulations of a 100 carbon ($X_n = 25$) PBD random copolymer of 50% trans and 50% cis units employing a quantum chemistry-based united atom potential function were performed at 353 K. The T_1 and NOE values obtained from simulation, as well as the center of mass diffusion coefficient and dynamic structure factor, were found to be in qualitative agreement with experiment. However, comparison of T_1 and NOE values for the various distinguishable resonances revealed that the local dynamics of the simulated chains were systematically too fast, whereas comparison with the center of mass diffusion coefficient revealed a similar trend in the chain dynamics. To improve agreement with experiment, (1) the chain length was increased to match the experimental M_z, (2) vinyl units groups were included in the chain microstructure, and (3) rotational energy barriers were increased by 0.4 kcal/mol in order to reduce the rate of conformational transitions. With these changes, dynamic properties from simulation were found to differ 20−30% or less from experiment, comparable to the agreement seen in previous simulations of polyethylene using a quantum chemistry-based united atom potential.

I. Introduction

Coordinated simulation and experimental studies, when performed on the same material under the same thermodynamic conditions, constitute a powerful method for gleaning molecular-level mechanistic detail of polymer dynamics. We have demonstrated the utility of this approach in our investigations of polyethylene (PE) and poly(ethylene oxide) (PEO) melts. In one study, the local conformational dynamics of *n*-$C_{44}H_{90}$ melts were studied via ^{13}C NMR spin−lattice relaxation techniques and compared with results of molecular dynamics simulations.[1,2] The T_1 spin−lattice relaxation times and nuclear Overhauser enhancement (NOE) values for *n*-$C_{44}H_{90}$ from simulation were in excellent agreement with experiment, demonstrating that the molecular dynamics simulations employing explicit (all atom) and united atom potentials based upon quantum chemistry can reproduce local dynamics in the PE melt with high accuracy. More recently, we have studied *n*-$C_{100}H_{202}$ melts using a combination of molecular dynamics and neutron scattering methods.[3−5] Comparison of the coherent single-chain dynamic structure factor obtained from simulations with neutron spin−echo (NSE) measurements yielded good agreement over the entire momentum transfer and time ranges studied for quantum chemistry-based explicit atom and united atom potentials. All atom simulations of PEO melts using a quantum chemistry-based potential function also yielded excellent agreement with experiment for ^{13}C NMR T_1 and NOE values as well as for the dielectric relaxation spectra.[6] These comparisons of experiment and simulation have led to important insights into the dynamics of polymer melts. For example, we were able to conclude that contributions of slow (compared to conformational dynamics) nonlocal chain motions are responsible for the deviation of the experimentally observed NOE values from extreme narrowing behavior for these unentangled melts.

Our studies of PE and PEO have been concerned primarily with melt dynamics. In the temperature range we have considered, chain relaxations are due to a combined $\alpha-\beta$ process. Of particular interest in polymer dynamics is the nature of the underlying molecular motions leading to the primary α and secondary β processes observed in glassy polymers,[7] and the rela-

10.1021/ma991130z CCC: $18.00
Published on Web 11/25/1999

tionship between these relaxations and the combined, high-temperature process. Despite extensive experimental and theoretical efforts, a fundamental mechanistic understanding of polymer relaxations lags far behind the phenomenological picture. It is the purpose of this work to begin to address these fundamental questions through a combined molecular dynamics simulation and experimental study of polybutadiene (PBD). Because of its simple chemical structure, wide range of microstructures, tightly controllable molecular weight distribution, and lack of crystallinity (for random copolymers, in contrast to PE and PEO, which readily crystallize), the dynamics of PBD have become the subject of extensive experimental study in recent years. The simple chemical structure and large body of experimental data make PBD an attractive candidate for atomistic simulations.

In previous work, we presented a quantum chemistry-based united atom force field for 1,4-polybutadiene.[8] In this work, we compare local and chain dynamics obtained from experiment and simulation of a low-molecular-weight PBD melt using this potential. One purpose of this comparison is to test the accuracy of the force field. On the basis of comparison of experiment and simulations, we have made modifications to the potential that are described below. The modified potential function, along with the quantum chemistry calculations on model compounds used in augmenting the potential to include vinyl groups, are presented here. Comparisons of experiment with simulations using the new potential function are presented. We have begun simulations of PBD at lower temperatures with the intent of gaining a molecular-level understanding of relaxation mechanisms in this representative glass-forming polymer, with particular emphasis on the dynamic region where the α and β relaxations split. Because of the decreased rate of local and chain dynamics at these lower temperatures, microsecond and longer trajectories will be required.

II. Experiment

Microstructure and Static Properties. Hydrogenated and deuterated PBD were synthesized by anionic polymerization of protonated and perdeuterated butadiene under identical conditions at room temperature. The initiator was *tert*-butyllithium at a concentration of 8×10^{-3} mol/L for both polymerizations. The microstructure, determined by ^{1}H and ^{13}C NMR measurements of the protonated material, was found to be 40% cis, 50% trans, and 10% 1,2-vinyl units. The NMR measurements were also used to determine the number-average degree of polymerization, $\langle X_n \rangle$, which was found to be 25.4. Including the initiator group, the resulting M_n is 1426 Da. Size-exclusion chromatography (SEC) was performed on the two polymers with tetrahydrofuran as the elution solvent. Five μ-styragel columns were used, covering a porosity range of 10^5−500 Å. Both materials revealed identical elution volumes, indicating the same degree of polymerization. On the basis of the polystyrene calibration of the SEC data, the polydispersity, M_w/M_n, was determined to be 1.06 for both materials. If a Poisson molecular weight distribution is assumed, $M_z/M_n = 1.12$, yielding $M_z = 1600$ Da. The *z*-average chain microstructure is therefore well-represented by a chain of 30 repeat unit, three of which are 1,2-vinyl, with a molecular weight of 1622 Da. This average chain has 114 backbone carbon atoms and 113 backbone bonds. As it is the *z*-average chain length that should be considered in analysis of neutron scattering data,[9] this average microstructure is considered in the analysis of the static and dynamic scattering data presented below. The single-chain static structure factor determined from SANS is well-represented by a Debye function with an root-mean-square (rms) radius of gyration of $R_g = 15.4$ Å. The density of the protonated material was found to be 0.843 g/cm^3 at 353 K.

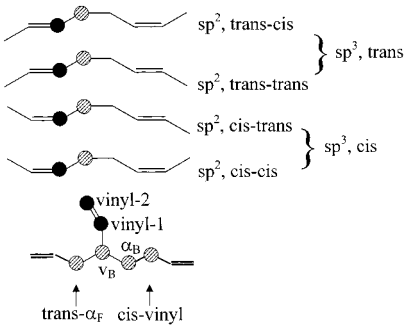

Figure 1. Local environments (microstructures) for the polybutadiene chains distinguished in ^{13}C NMR measurements. Filled circles denote sp^2 nuclei, and hatched circles denote sp^3 nuclei. Trans α_F indicates that only corresponding resonances for vinyl groups preceded by a trans-1,4 unit are resolved, whereas cis−vinyl indicates that only corresponding resonances for vinyl groups followed by a cis-1,4 unit are resolved.

Local Dynamics. ^{13}C NMR spin−lattice relaxation studies were performed at a 300 MHz proton Larmor frequency over a temperature range of 303−357 K. NOE values were also obtained over the same temperature range. Twelve separate resonances, assigned as illustrated in Figure 1, were considered. Because only ^{13}C−^{1}H dipolar relaxation is significant, the spin−lattice relaxation time T_1 and NOE value obtained from the ^{13}C are related to the molecular dynamics of the polymer through the following relationships[10]

$$\frac{1}{n{T_1}^k} = K[J^k(\omega_H - \omega_C) + 3J^k(\omega_C) + 6J(\omega_H + \omega_C)] \quad (1)$$

$$\mathrm{NOE}^k = 1 + \frac{\gamma_H}{\gamma_C}\frac{6J^k(\omega_H + \omega_C) - J^k(\omega_H - \omega_C)}{J^k(\omega_H - \omega_C) + 3J^k(\omega_C) + 6J^k(\omega_H + \omega_C)} \quad (2)$$

where n is the number of attached protons, ω_H and ω_C are the resonance (angular) frequencies of the ^{13}C and ^{1}H nuclei, respectively, and γ_H and γ_C are the corresponding gyromagnetic ratios. The superscript k indicates a differentiable resonances due to local environment (see Figure 1). The constant K is given by[10]

$$K = \frac{\hbar^2 {\mu_0}^2 {\gamma_H}^2 {\gamma_C}^2}{160\pi^2 \langle {r_{CH}}^3 \rangle^2} \quad (3)$$

where μ_0 is the permittivity of free space and r_{CH} is the carbon−hydrogen bond length. K assumes values of 2.29×10^9 and 2.42×10^9 s^{-2} for sp^3 and sp^2 nuclei, respectively.[10] The spectral density function $J(\omega)$ is given as[10]

$$J^k(\omega) = \frac{1}{2}\int_{-\infty}^{\infty} {P_2}^k(t) e^{i\omega t}\, dt \quad (4)$$

where

$$ {P_2}^k(t) = \frac{1}{2}\{3\langle [\mathbf{e}_{CH}{}^k(t) \cdot \mathbf{e}_{CH}{}^k(0)]^2 \rangle - 1\} \quad (5)$$

Here, $\mathbf{e}_{CH}$ is a unit vector along a particular C−H bond. As discussed previously,[1,2,6,11] simulations have revealed that the decay of the C−H vector autocorrelation function (eq 5) in polymer melts occurs primarily, but not entirely, as the result of local conformational changes. Consequently, ^{13}C NMR spin−lattice relaxation times and NOE values are predominantly dependent upon local dynamics.

The measured T_1 and NOE values for PBD at 353 K, given in Table 1, are qualitatively consistent with previous work on

Table 1. T_1 and NOE Values for Various Nuclei at 353 K

	τ_c (ps)[b]	nT_1 (s)[c]			NOE		
nuclei[a]	exp	exp	FF	FF mod	exp	FF	FF mod
t−cis [sp²]	23 (30)	1.8 ± 0.05	3.3	1.9	2.4 ± 0.1	2.8	2.5
t−*t* [sp²]	26 (31)	1.6 ± 0.05	3.2	1.8	2.4 ± 0.1	2.8	2.5
cis−cis [sp²]	24 (26)	1.7 ± 0.05	3.3	1.7	2.8 ± 0.1	3.0	2.9
cis−*t* [sp²]	30 (28)	1.4 ± 0.05	3.0	1.5	2.8 ± 0.1	3.0	2.9
t [sp³]	26 (25)	1.7 ± 0.05	3.6	1.8	2.6 ± 0.1	2.9	2.8
cis [sp³]	19 (22)	2.3 ± 0.05	4.4	2.2	2.8 ± 0.1	2.9	2.8
v_B (branch) [sp³]	44 (40)	1.0 ± 0.1		1.2	2.8 ± 0.2		2.8
trans α_F [sp³]	44 (50)	1.0 ± 0.1		1.2	2.7 ± 0.2		2.7
α_B [sp³]	34 (43)	1.3 ± 0.1		1.4	2.8 ± 0.2		2.7
vinyl 1 [sp²]	23 (10)	1.8 ± 0.1		4.4	2.5 ± 0.2		3.0
vinyl 2 [sp²]	32 (26)	1.3 ± 0.1		1.8	2.7 ± 0.2		2.8
cis−vinyl [sp³]	28 (40)	1.5 ± 0.1		1.3	2.7 ± 0.2		2.7

[a] See Figure 1 for assignments. [b] Assumes extreme narrowing behavior (eq 6). [c] Here, *n* is the number of attached hydrogen atoms. FF denotes the original potential function from Smith and Paul,[8] whereas FF mod denotes the modified potential function of this work. [d] Numbers in parentheses are from simulations using FF mod (see Table 2).

high-molecular-weight PBD.[12] The C−H vector correlation time, defined as the time integral of eq 5, can be estimated using the relationship[1]

$$\tau_c = \frac{1}{10KnT_1} \tag{6}$$

This relationship assumes extreme narrowing behavior (NOE ≈ 3). Hence, the correlation times given in Table 1, obtained by applying eq 6 to the experimental data, give a qualitative measure of the relaxation time for C−H vectors associated with the various nuclei. The longest (apparent) relaxation times are seen for the sp³ nuclei near the vinyl side groups, whereas the shortest time is seen for the sp³ nuclei in a cis unit (not neighboring a vinyl unit). NOE values for the sp² carbons in trans units (trans−trans and trans−cis environments) as well as for the vinyl-1 sp² carbon are significantly reduced from 3, indicating that nonlocal contributions to the decay of the C−H vector P_2 autocorrelation function may be important for these nuclei.

Chain Dynamics. Single-chain dynamics were investigated by NSE spectroscopy. A liquid mixture of 10% or 15% hydrogenated PBD in a 90% or 85% deuterated PBD at 80 °C was used as the sample, with pure deuterated PBD serving as a background. The samples were contained in niobium cuvettes providing a sample area of 30 × 30 mm² with a thickness of 4 mm. The NSE experiments were performed at the new NSE-FRJ2 spectrometer at Jülich,[13] by using a neutron wavelength band centered at $\lambda = 8$ Å with a width of 10% fwhm. Relaxation functions $\tilde{S}(\mathbf{q}, t) = S(\mathbf{q}, t)/S(\mathbf{q}, 0)$ were sampled at 14 time values of 0.1 ns ≤ *t* ≤ 22 ns. Data were taken at seven different scattering angle settings corresponding to $q = 0.05$ (4.1), 0.08 (4.6), 0.10 (5.1), 0.14 (5.7), 0.20 (6.7), 0.24 (7.8), and 0.3 (7.8), with the numbers in brackets denoting the measuring times in hours. A completely analogous set of data has been taken for the background sample and was subtracted from the sample data according to the procedure described previously.[13] Instrumental resolution effects have been accounted for using reference scans from purely elastic scatterers (MgO powder for $q = 0.05$ Å^{-1} and microcrystalline carbon (Carbopack) for the higher *q* values). Due to the use of a large area detector, data were collected over range of up to five *q* values between $q - 0.023$ Å^{-1} and $q + 0.023$ Å^{-1} simultaneously and were averaged in order to obtain better statistical accuracy. These data are compared with predictions of simulation and theory determined without averaging.

The normalized single-chain intermediate coherent dynamic structure factor is defined as

$$\tilde{S}(\mathbf{q}, t) = \frac{S(\mathbf{q}, t)}{S(\mathbf{q}, 0)} = \sum_{ij} \exp[i\mathbf{q} \cdot \mathbf{r}_{ij}(t)] / \sum_{ij} \exp[i\mathbf{q} \cdot \mathbf{r}_{ij}(0)] \tag{7}$$

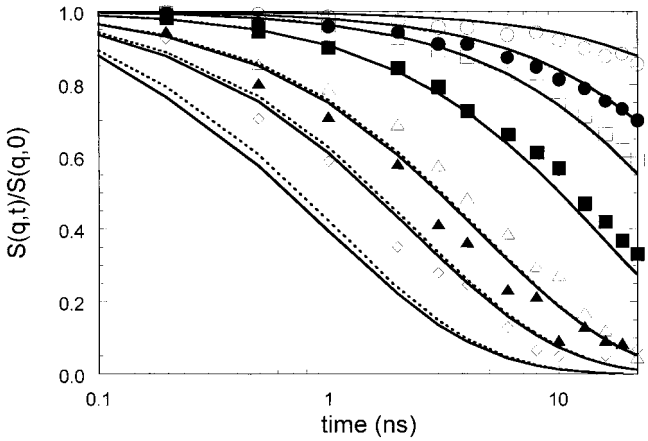

Figure 2. Single-chain coherent intermediate dynamic structure factor for polybutadiene at 353 K. Symbols ($q = 0.05$ (open circle), 0.08, 0.10, 0.14, 0.20, 0.24, and 0.30 (diamond) Å^{-1}) are from NSE measurements. Solid lines are predictions from the Rouse model, and the dashed lines are from a wormlike chain model. For both models, $D = 2.3 \times 10^{-7}$ cm²/s.

where $\mathbf{q}$ is the scattering vector and $\mathbf{r}_{ij}(t) = \mathbf{r}_i(t) - \mathbf{r}_j(0)$ is the vector between scattering centers (hydrogen atoms) *i* and *j* at time *t* and 0, respectively, with *i* and *j* belonging to the same chain. For an isotropic (melt) sample eq 7 reduces to

$$\tilde{S}(q, t) = \sum_{ij} \sin[qr_{ij}(t)]/qr_{ij}(t) / \sum_{ij} \sin[qr_{ij}(0)]/qr_{ij}(0) \tag{8}$$

where $r_{ij}(t)$ is the magnitude of $\mathbf{r}_{ij}(t)$.

$\tilde{S}(q, t)$ from NSE measurements are shown in Figure 2. When $q^2\langle R_e^2\rangle \ll 1$, one can observe only the overall diffusion of the chain molecules, and

$$\tilde{S}(q, t) = \exp(-q^2 D_{NSE} t) \tag{9}$$

where D_{NSE} is the (apparent) center of mass self-diffusion coefficient for the chains. D_{NSE} is equal to the true center of mass diffusion coefficient only when *q* is sufficiently small such that contributions from internal modes can be neglected. The contributions of smaller wavelength (internal) modes of the polymer to the decay of the structure factor can be approximated by assuming that the Rouse model[14] describes motions in our unentangled melt. In this case, the dynamic structure factor is given by[4]

$$\tilde{S}(q, t) = \frac{1}{N_{seg}} \exp\{-q^2 D_R t\} \sum_{(n,m=1)}^{N_{seg}} \times \exp\left\{-\frac{q^2\sigma^2}{6}|n - m| - \frac{2q^2\sigma^2 N_{seg}}{3\pi^2} \sum_{N_{seg}}^{p=1} \frac{1}{p^2} \cos\left(\frac{p\pi n}{N_{seg}}\right) \times \cos\left(\frac{p\pi n}{N_{seg}}\right)[1 - \exp(-tp^2/\tau_R)]\right\} \tag{10}$$

where N_{seg} is the number of statistical segments in the chains, σ is the statistical segment length, D_R is the center of mass diffusion coefficient, and τ_R is the Rouse time. Because $N_{seg}\sigma^2 = 6\langle R_g^2\rangle$ and assuming $N_{seg}\sigma = L_c$, where L_c is the contour length of the chain, we obtain $N_{seg} = N/C_N = 20$ and $\sigma = 8.4$ Å for the PBD chains. The characteristic ratio is defined as $C_N = \langle R^2\rangle/Nl^2$, where l^2 is the average squared backbone bond length and *N* is the number of backbone bonds. Because $\langle R_g^2\rangle$ is known for our chains, the only adjustable parameter in eq 10 is D_R, as the Rouse time is given by[14]

$$\tau_R = \frac{2\langle R_g^2\rangle}{\pi^2 D_R} \tag{11}$$

The best fit of the Rouse model (eq 10) to experiment is shown in Figure 2, where a value of $D_R = 2.3 \times 10^{-7}$ cm^2/s has been used, yielding a Rouse time of $\tau_R = 21$ ns. The fit somewhat underestimates the decay for small q in order to compensate for the too-fast decay of the Rouse model at larger q. Using eq 9 to determine the diffusion coefficient at $q = 0.05$ Å^{-1} results in a value of $D_{NSE} = 2.8 \times 10^{-7}$ cm^2/s and a Rouse time of $\tau_R = 17$ ns. As eq 9 neglects all contributions of internal modes, this value can be considered an upper limit for the diffusion coefficient. For the larger momentum transfers investigated, the contribution of the internal modes is particularly important. In these cases, the Rouse model, as was found previously for an unentangled polyethylene melt,[4] fails to reproduce the experimentally observed $\tilde{S}(q, t)$, as shown in Figure 2.

It has been claimed that a semiflexible chain model[15] that accounts for the effects of chain stiffness on scales comparable to the persistence length does a much better job in reproducing experimental $\tilde{S}(q, t)$ at short times and large momentum transfers than the Rouse model for polymer melts. In addition to the center of mass diffusion coefficient, this model has two additional adjustable parameter; the contour length L_c and the persistence length L_p. The contour length appropriate for random-walk chains[16] is $L_c = Nl$, where N is the number of backbone bonds and l is the average bond length. By the use of quantum chemistry values for the bond lengths,[8] $L_c = 167$ Å for the PBD chains with $M_z = 1600$. The semiflexible chain model predicts the mean-square end-to-end distance and mean-square radius of gyration as[15,16]

$$\langle R_e^2 \rangle = 2L_cL_p - 2L_p2[1 - \exp(-L_c/L_p)] \qquad (12)$$

and

$$\langle R_g^2 \rangle = L_cL_p/3 - L_p^2 + 2L_p^3/L_c + 2L_p^4/L_c^2[1 - \exp(-L_c/L_p)] \qquad (13)$$

as a function of the parameters L_c and L_p. Our simulations, for which $\tilde{S}(q, t)$ is in good agreement with experiment (see below), yield $\langle R_e^2 \rangle / \langle R_g^2 \rangle = 1445$ Å^2/229 Å^2 = 6.3. By the use of $L_c = 167$ Å, a value of $L_p = 4.56$ Å yields $\langle R_e^2 \rangle / \langle R_g^2 \rangle = 1481$ Å^2/234 Å^2 = 6.3, in good agreement with the real (simulation) chains. (Note that the experimental value is $\langle R_g^2 \rangle = 234$ Å^2.) The resulting $\tilde{S}(q, t)$ for the semiflexible chain[15] using these parameters, which provide an accurate representation of the chain conformations on length scales larger than the persistence length, is shown in Figure 2 (dashed lines). The values are nearly indistinguishable from the Rouse predictions.

To improve agreement between the semiflexible chain predictions and experiment at large q, it is necessary to "stiffen" the chains by increasing the persistence length. To retain an accurate value for $\langle R_g^2 \rangle$, which is known experimentally, the contour length must be simultaneously reduced (via eq 13). For example, a much improved representation of $\tilde{S}(q, t)$ is obtained with $L_p = 9.3$ Å and $L_c = 84.5$ Å. (Note that even stiffer chains can provide further improvement in $\tilde{S}(q, t)$). For these parameters, $\langle R_e^2 \rangle / \langle R_g^2 \rangle = 1414$ Å^2/194 Å^2 = 7.3. Hence, although the "real" chains are nearly Gaussian, the semiflexible chains that yield a reasonable representation of the experimental $\tilde{S}(q, t)$ for larger q values are too short and stiff to be Gaussian. The resulting parameters (contour and persistence length) provide an inaccurate description of chain conformations on length scales longer than the persistence length.

III. Molecular Dynamics Simulations

Microstructure, Methodology, and Static Properties. We have performed simulations of a PBD melt using the quantum chemistry-based united atom potential described elsewhere.[8] For these simulations (which preceded the synthesis of the PBD), we made the assumption that the chains to be synthesized would be 100 backbone carbons in length ($M = 1350$ Da) with a microstructure of 50% trans and 50% cis units. The microstructure of the 40 chains (4000 total united atoms) was generated using a Monte Carlo procedure that assumed Bernoulli chain statistics. The overall system had a trans fraction of 50.7%, exactly matched the expected dyad (trans−trans, trans−cis, and so on) fractions, and matched the expected triad fractions within 1% for each triad. The chains were initially placed on a low-density lattice with periodic boundary conditions at 1000 K. After 100 ps, the temperature was reduced to 500 K. The system was run for 2 ns while the volume was decreased to yield an average pressure of 1 atm. The temperature was reduced to 353 K, and the density at 1 atm was determined through a series of NPT runs performed over 2 ns. The density was found to be 0.865 g/cm^3, with a corresponding periodic box size of 47.02 Å. This is in good agreement with the experimental value of 0.843 g/cm^3. To some extent, the slightly lower density of the experimental system may be due to the large *tert*-butyl initiator groups. The system was further equilibrated at this volume for 5 ns. A 16 ns trajectory was subsequently computed. During the simulations, bond lengths were constrained using the SHAKE algorithm, and a time step of 1 fs was employed. We obtained an rms radius of gyration of 13.2 Å and an rms end-to-end distance of $R_e = 32.3$ Å for the $M = 1350$ Da chains. The radius of gyration is significantly less than the value of $R_g = 15.4$ Å obtained experimentally, reflecting the fact that the simulated chains are shorter than the z-averaged chain length ($M_z = 1600$, approximately 114 backbone carbons) obtained from the scattering experiments.

Local Dynamics. The C−H vector $P_2(t)$ autocorrelation functions for the six nuclei illustrated in Figure 1 not involving the vinyl side groups were determined from the simulation trajectories. To accomplish this, it was necessary to calculate the positions of the hydrogen atoms from the stored united atom (carbon) positions. To best represent the molecular geometries obtained from quantum chemistry calculations, the hydrogen atoms attached to sp^2 carbons were placed along the bisector of the alkene and allyl bonds. The hydrogen atoms attached to sp^3 carbons were placed such that the bisector of the H−C−H valence angle (107° for trans units and 106.6° for cis units) was in the C−C−C plane. It should be noted that the calculated P_2 functions are somewhat sensitive to the placement of the hydrogen atoms, and care must be taken to place them accurately. As in our previous work[1,6] we represented the C−H vector $P_2(t)$ functions obtained form simulations as a sum of a stretched exponential term (KWW equation) associated with local (conformational) contributions to the relaxation and a single, long-relaxation time exponential previously associated with motions of the chain backbone.[1,2] Hence,

$$P_2^{fit}(t) = A \exp[-(t/\tau_{KWW})^{\beta}] + (1 - A)\exp(-t/\tau_{tail}) \qquad (14)$$

Parameters for the empirical fits as well as the correlation time τ_c (time integral of the correlation function from the fit of eq 14) are given in Table 2. From the fits, the spectral density is easily calculated using eq 4, and subsequently, eqs 1 and 2 can be used to calculate the T_1 and NOE values. The T_1 and NOE values obtained from simulation are compared with experimental values in Table 1. Values from simulation are

Table 2. Fit Parameters and Correlations Times for the Various C−H Vector $P_2(t)$ Autocorrelation Functions at 353 K

	FF[a]					FF modified[b]				
nuclei	τ (ps)	β	A	τ_{tail} (ps)	τ_c (ps)	τ (ps)	β	A	τ_{tail} (ps)	τ_c (ps)
t−cis [sp^2]	1.7	0.378	0.976	330	14	2.9	0.377	0.970	570	30
t−t [sp^2]	2.2	0.383	0.981	370	15	3.7	0.378	0.974	640	31
cis−cis [sp^2]	5.3	0.458	1.00		13	10.3	0.450	1.00		26
cis−t [sp^2]	6.1	0.467	1.00		14	11.5	0.450	1.00		28
t [sp^3]	3.1	0.386	0.992	100	12	6.4	0.386	0.989	170	25
cis [sp^3]	2.6	0.375	0.996	80	11	5.1	0.372	0.996	250	22
v_B (branch) [sp^3]						16.2	0.453	1.00		40
trans α_F [sp^3]						11.9	0.419	0.98	800	50
α_B [sp^3]						10.7	0.424	0.99	1250	43
vinyl 1 [sp^2]						0.7	0.431	0.88	70	10
vinyl 2 [sp^2]						4.9	0.349	0.98	70	26
cis−vinyl [sp^2]						9.4	0.410	0.98	590	40

[a] Original potential function from Smith and Paul.[8] [b] Modified potential function of this work.

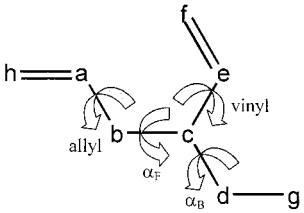

Figure 3. 3-Ethyl-1,5-hexadiene, the model compound used in quantum chemistry calculations for parametrizing vinyl torsions. Dihedrals and backbone atoms used in defining dihedral angles are labeled.

systematically larger than those observed experimentally, indicating that the C−H vector $P_2(t)$ autocorrelation functions for all C−H vectors decay too rapidly in the simulated system compared with the expected behavior. This trend can also be seen by comparing the τ_c values from simulations (Table 2) with the apparent values from experiment (Table 1).

We can directly monitor conformational dynamics through the dihedral autocorrelation function, defined as

$$P(t) = \frac{\langle \cos\phi(t) \cos\phi(0)\rangle - \langle \cos\phi(0)\rangle^2}{\langle \cos\phi(0) \cos\phi(0)\rangle - \langle \cos\phi(0)\rangle^2} \qquad (15)$$

where ϕ is the dihedral angle. The various types of dihedrals for the vinyl unit are illustrated in Figure 3. For cis and trans units, the dihedrals adjacent to the double bond are referred to as cis allyl and trans allyl, respectively. The dihedral connecting two allyl bonds is referred to as β. The $P(t)$ autocorrelation functions for trans and cis allyl dihedrals, as well as that for the β dihedral, are shown in Figure 4. The time integral of eq 15 yields the torsional autocorrelation times, which are approximately 3, 6, and 40 ps, for the allyl trans, allyl cis, and β bonds, respectively. The torsional autocorrelation time for the allyl trans dihedral is relatively short, consistent with the low (2−2.5 kcal/mol) rotational energy barriers for this bond.[8] The torsional autocorrelation function for the allyl cis dihedral initially decays more rapidly than that of the allyl trans bond due to the low $s^+\_s^-$ energy (slightly greater than 1 kcal/mol;[8] see footnotes to Table 3 for definitions of rotational states) and more slowly at longer times due to the high energy of the cis conformation of the allyl cis dihedral. The correlation time for the β dihedral is about an order of magnitude greater than that for the allyl bonds, consistent with the higher rotational energy barriers (3.5 to 4.5 kcal/mol)[8] for this bond. The autocorrelation times for the C−H vectors given in Table 2 lie between those for the allyl and β dihedrals. The correspondence of the correlation times for the C−H vector $P_2(t)$ and torsional autocorrelation functions indicates that the poor agreement between simulation and experiment for T_1 and NOE can be associated to a large degree with a too-fast rate of conformational transitions in the simulated system.

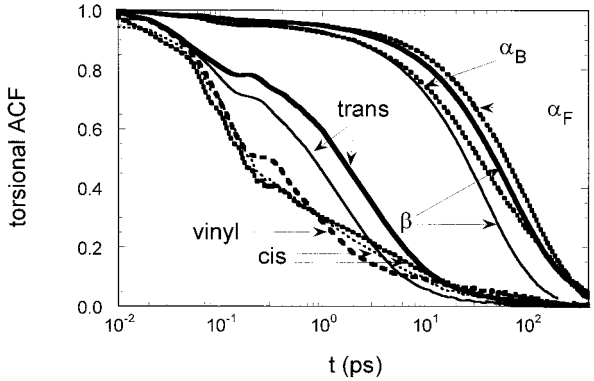

Figure 4. Dihedral autocorrelation functions for the original potential function (normal lines) and the modified potential function (heavy lines). The heavy dotted lines labelled α_B, α_F, and vinyl are only present in the modified force field.

Chain Dynamics. The $\tilde{S}(q, t)$ data from MD simulations for q = 0.05, 0.08, and 0.10 Å^{-1} can be well represented by eq 10 with $D_R = 5.6 \times 10^{-7}$ cm^2/s, in good agreement with the center of mass diffusion coefficient of $D_{cm} = 5.8 \times 10^{-7}$ cm^2/s obtained directly from simulation employing the relationship

$$D_{cm} = \lim_{t\to\infty} \langle R_{cm}^2 \rangle / 6t \qquad (16)$$

where $\langle R_{cm}^2 \rangle$ is the mean-square center of mass displacement of a chain. These values are significantly larger than the value of $D_R = 2.3 \times 10^{-7}$ cm^2/s obtained from fitting the low q experimental $\tilde{S}(q, t)$ with eq 10 or $D_{NSE} = 2.8 \times 10^{-7}$ cm^2/s from eq 9. By plotting $\tilde{S}(q, t)$ from experiment and simulation as a function of $D_R t$, differences in the center of mass diffusion coefficient can be scaled out. This has been done in Figure 5. Agreement between simulation and experiment is better than what was found for the Rouse model (Figure 1) for the larger q values. In our previous comparison of $\tilde{S}(q, t)$ for n-$C_{100}H_{202}$ melts,[4] somewhat better agreement between experiment and simulation was seen at short times and large q values, where the smaller wavelength modes make a more important contribution. It is simple

Table 3. Geometries and Energies of Low-Energy Conformers and Rotational Energy Barriers in EHD

	geometry[b]				energy (kcal/mol)[b,c]		
conformer[a]	allyl (h−a−b−c)	α_F (a−b−c−d)	α_B (b−c−d−g)	vinyl (b−c−e−f)	SCF	MP2	FF mod
			Low-Energy Conformers				
s^+tts^+	126.7	173.4	−171.5	120.5	0.00	0.00	0.0
$s^+\bar{g}ts^+$		−64.1	−169.0	108.8	0.60	0.16	0.1
s^+gts^+	112.3	64.6	−173.9	114.9	0.41	0.43	0.5
s^+tgs^+	126.9	175.8	−64.7	123.4	0.80	0.90	0.7
$s^+\bar{g}s^+$	122.1	−61.1	−61.6	110.3	1.16	0.68	1.0
$s^+\bar{g}s^-$	126.9	−60.0	−60.7	−123.1	1.66	0.90	1.3
$s^+t\bar{g}s^+$	125.7	168.0	63.4	126.9	1.34	1.25	0.8
$s^+\bar{g}ts^-$	123.2	−61.1	−161.1	−114.5	2.02	1.35	1.3
$s^+g\bar{g}s^+$	112.1	57.1	59.4	120.3	1.62	1.36	1.4
$s^+g\bar{g}cis$	111.6	57.3	59.9	−4.6	2.19	1.54	2.3
s^+tts^-	122.4	170.0	−165.2	−108.9	2.01	1.70	1.7
$s^+\bar{g}cis$	129.3	−54.9	−60.4	7.2	2.61	1.72	2.2
s^+tgs^-	122.5	168.6	−66.9	−119.7	1.94	1.75	1.2
$s^+t\bar{g}cis$	136.6	161.6	61.9	−7.3	2.66	2.13	2.1
s^+gtcis	111.6	64.9	−174.3	−14.2	2.41	2.13	2.3
$s^+t\bar{g}s^-$	123.2	161.8	56.3	−140.3	2.77	2.27	2.2
s^+gts^-		68.2	−166.1	−108.1	2.50	2.30	2.2
			α_F Rotational Barriers				
$s^+[g\_t]ts^+$	119.6	116.3	−172.8	114.7	2.96	3.13	3.2
$s^+[t\_\bar{g}]ts^+$	121.0	−123.2	−172.0	116.9	4.74	4.18	4.1
$s^+[g\_\bar{g}]ts^+$	120.7	−3.7	−169.6	113.6	5.49	5.05	5.0
			Vinyl Rotational Barriers				
$s^+\bar{g}g[s^+\_s^-]$	128.0	−58.3	−60.4	179.5	3.85	2.60	2.5
$s^+\bar{g}g[s^+\_cis]$	126.2	−60.1	−60.2	45.3	3.37	3.03	2.6
$s^+\bar{g}g[s^-\_cis]$	120.2	−51.5	−61.7	−50.8	5.80	4.73	4.7

[a] s (skew)$^+$ = +120°, s (skew)$^-$ = −120°, t (trans) = 180°, cis = 0°, g = gauche with respect to the backbone, trans with respect to the side group, and $\bar{g}$ = gauche with respect to the backbone and side group. [b] From MP2/6-311G** geometries. See Figure 1 for sequence definition. [c] Using a 6-311G** basis set, relative to the s^+tts^+ conformer.

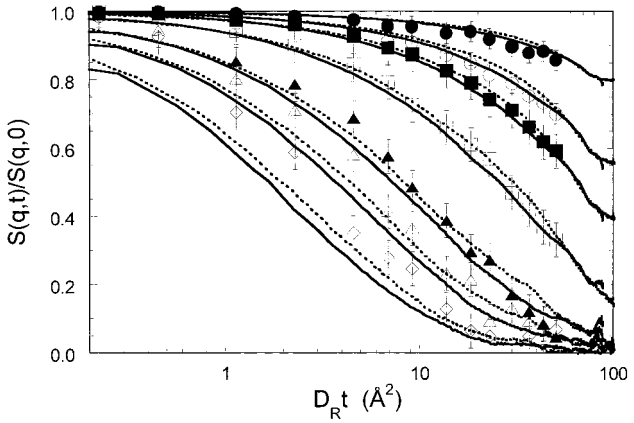

Figure 5. Single-chain coherent intermediate dynamic structure factor for PBD at 353 K as a function of scaled time. Symbols (q = 0.05 (filled circles), 0.08, 0.10, 0.14, 0.20, 0.24, and 0.30 (diamonds) Å^{-1}) are from NSE measurements, and lines are from simulation. Solid lines are from the original force field, and dashed lines are from the modified force field.

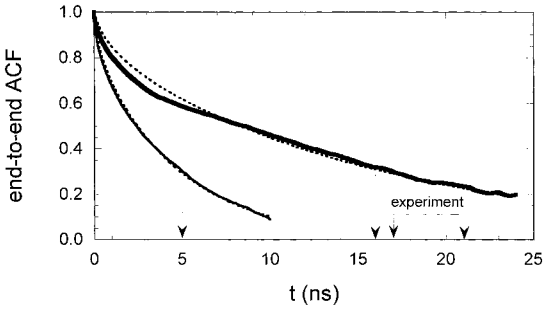

Figure 6. End-to-end vector autocorrelation function for 1,4-polybutadiene from molecular dynamics simulations for the original force field (thin line, fast relaxation) and the modified force field (thick line, slow relaxation). The corresponding dashed lines are from fitting of the Rouse model. Rouse times for both potentials as well as the upper and lower bounds for the Rouse time from experiment are also indicated by the arrows.

to show that in scaled time units, the Rouse model yields[14]

$$\frac{\tau_1}{t_2} = \frac{N_1}{N_2} \tag{17}$$

where τ is the relaxation time (in scaled time units) for any mode $p > 0$, N is the number of statistical segments, and the subscript i denotes a chain of length N_i statistical segments. Hence, we expect $\tau_{sim} < \tau_{exp}$ simply because the simulation chains are too short, consistent with the behavior observed in Figure 5 for short times and large q values.

We can also examine chain dynamics by investigating the relaxation time for the end-to-end vector of the chain. For Rouse chains, the $P_1(t)$ autocorrelation function for the end-to-end vector (normalized to $P_1(0) = 1$) is given by[14]

$$P_1(t) = \sum_{p=1,3,5} \frac{8}{p^2\pi^2} \exp[-tp^2/\tau_R] \tag{18}$$

where τ_R is the Rouse time given by eq 11. The simulation end-to-end $P_1(t)$ is fit very well by eq 18 with τ_R = 5 ns, as demonstrated in Figure 6. Equation 11 yields a value of τ_R = 6 ns for the simulation chains. These times are much shorter than the Rouse time of τ_R = 17−21 ns obtained from the experimental data.

IV. Modified Force Field

On the basis of the comparison between simulations and experiment for R_g, ^{13}C T_1 and NOE values, and $\tilde{S}(q,$

t), we conclude that (1) the simulation chains are too short and (2) the rate of conformational transitions in the simulation melt is too high. The appropriate chain length for reproducing neutron scattering measurements is the *z*-average chain length, which, as described above, can be represented as a chain with 114 backbone carbons as opposed to the 100 carbons used in the initial simulations. By increasing the length of the chains to match that of the experimental chains, we can expect to improve agreement with experimental $\tilde{S}(q, t)$ on a scaled time basis and to reduce D_{cm}. However, increasing chain length will have little influence on the rate of conformational transitions. Therefore, to improve agreement with experiment for T_1 and NOE, it is necessary to modify the potential in order to increase rotational energy barriers. In comparison of united atom and explicit atom simulations of polyethylene using potentials that reproduce the conformational energetics in butane as determined from high-level quantum chemistry calculations, it was found that the rate of conformational transitions was significantly greater in the united atom simulations.[2] When the barrier for trans-to-gauche transitions was increased by 0.3 kcal/mol over the value obtained for quantum chemistry studies, a good representation of local conformational (and chain) dynamics was obtained using the united atom model. It is worth noting that the explicit atom potential reproduced experimental data well without modification. Hence, the too-fast rate of conformational transitions (the need for increased rotational energy barriers) appears to be an artifact of the united atom representation and not a deficiency in the quantum chemistry energies. The slowing of conformational dynamics resulting from increased rotational energy barriers will also influence chain dynamics by decreasing D_{cm} through an increase in the monomer friction coefficient. This should improve agreement between simulation and experiment for $\tilde{S}(q, t)$, and the combination of longer chains and decreased D_{cm} will improve agreement for the Rouse time.

In addition to chain length, our simulated chains differ from the experimental chains in microstructure: specifically, we have not included vinyl units in the simulated chains. At low vinyl content, the influence of vinyl units on dynamics is unknown. However, a study of the glass-transition temperature as a function of microstructure (vinyl content) revealed a strong dependence for higher vinyl content microstructures, with the glass-transition temperature increasing dramatically with increasing vinyl content.[17] To include 1,2-vinyl units in the simulations, it is necessary to accurately reproduce conformational energetics for the torsions shown for the model compound 3-ethyl-1,5-hexadiene (EHD), illustrated in Figure 3, in addition to those previously parametrized. (We neglect vinyl−vinyl dyads due to the low frequency of these groups in the random copolymer). For this purpose, we have performed quantum chemistry calculations on EHD using the quantum chemistry package *Gaussian 98*.[18] As in our previous study of PBD model compounds, we performed geometry optimization at the SCF/6-311G** level with subsequent single-point energy calculations at the MP2/6-311G** level. The relative energies and geometries of the most important conformers and rotational energy barriers in EHD are given in Table 3. As was seen previously for other PBD model compounds,[8] electron correlation significantly influences the relative conformer energies in EHD. Employing previously developed nonbonded and valence potentials,[8] the torsional parameters for the new dihedrals were adjusted to give optimal agreement between quantum chemistry and force field predictions for conformational energies and rotational energy barriers for the model compounds. The ability of the force field to reproduce the quantum chemistry conformational energies and rotational energy barriers is demonstrated in Table 3. The agreement with quantum chemistry is reasonable. Table 4 gives the corresponding force field parameters.

Table 4. Torsional Parameters for Polybutadiene

		parameters (kcal/mol)[b]					
torsion	sequence[a]	k_1	k_2	k_3	k_4	k_4	k_6
α_F	a−b−c−d	−0.95	−0.58	−2.01	0.23	0.43	−0.27
α_F	a−b−c−e	0.49	0.08	−2.01	0.25	0.52	−0.27
α_B	b−c−d−g	−2.60	−1.05	−2.27	−0.28	−0.12	−0.26
α_B	e−c−d−g	−1.92	−1.07	−2.27	0.07	0.38	−0.26
vinyl	f−e−c−b	−1.92	0.32	0.75	−0.23	−0.08	−0.09
vinyl	f−e−c−d	−1.52	0.72	0.75	−0.15	0.11	−0.09
cis (allyl)		0.86	−0.04	1.16	0.16	0.38	−0.12
trans (allyl)		−0.24	−0.73	2.38	0.08	0.09	−0.06
β		−0.99	−0.62	−4.04	−0.07	−0.25	−0.19

[a] See Figure 3. [b] $E = {}^1/_2 \sum_{n=1}^{6} k_n[1 - \cos n\phi]$.

The final modification to the system involves reduction of the rates of torsional transitions for the allyl and β dihedrals in the united atom PBD (see discussion above). To accomplish this, we increased the barriers (3-fold dihedral parameters) for all transitions of the allyl trans and β dihedrals by 0.4 kcal/mol. For the allyl cis bond, we additionally modified the potential so as to minimize the impact of an increased $s^+\_s^-$ energy (see Table 3 for definition of conformational states), or trans barrier, on the conformational population in the vicinity of the trans angle. The modified torsional potentials for these dihedrals is also given in Table 4.

V. Simulations-Modified Potential

We generated a new random copolymer system of 40 chains, each comprised of 30 units with a microstructure of 40/50/10 cis/trans/vinyl without vinyl−vinyl dyads. Hence, each chain contains three vinyl units and 114 backbone carbons. These chains have a molecular weight of 1622 Da, in agreement with the $M_z = 1600$ Da of the synthesized chains. The systems were generated and equilibrated according to the procedure described in section II. Following 10 ns of equilibration, a 30 ns constant-volume trajectory was generated.

Thermodynamic and Static Properties. Molecular dynamics simulations analogous to those performed for the original force field were performed using the modified potential and the 40/50/10 cis/trans/vinyl chains system described above. For these simulations, a reversible multiple-time-step algorithm was employed[19] using the SHAKE algorithm to constraint bond lengths. An inner time step of 1 fs was used for bonded interactions and an outer time step of 5 fs was employed for nonbonded interactions. Constant-pressure simulations yielded a density of 0.880 g/cm^3 at 353 K. This density is slightly higher than that obtained for the chains without vinyl groups. To obtain a reasonable representation of the conformational energies and rotational energy barriers in EHD, we found it necessary to use the nonbonded potential for the smaller $C(sp^2)H-$ group to represent the $C(sp^2)H_2-$ group (center "f" in Figure 3). As a consequence, the vinyl group is effectively too small in terms of intermolecular nonbonded

interactions, accounting, we believe, for the higher density of the chains 40/50/10 chains compared to the 50/50 chains initially simulated. An rms radius of gyration of $R_g = 15.1$ Å was obtained for the 1622 Da chains, in much better agreement with the experimental value of 15.4 Å.

Local Dynamics. The ^{13}C NMR T_1 spin−lattice relaxation times and NOE values were determined by applying eq 4 to the fit of the C−H vector $P_2(t)$ autocorrelation functions obtained from eq 14 for the various carbons. The T_1 and NOE values are given in Table 1, and the fit parameters and correlation times are given in Table 2. Unlike simulations with the original force field and shorter chains, the T_1 and NOE values are in excellent agreement with experiment for the various carbons, indicating that the force field is faithfully reproducing local dynamics in PBD. The exception to this agreement is for the vinyl-1 and vinyl-2 sp^2 nuclei. The T_1 and NOE values for these carbons are strongly influenced by rotation of the vinyl side group. For the values reported in Table 1, we have not increased the rotational energy barrier for the vinyl group from that obtained from fitting the quantum chemistry as was done for the backbone dihedrals. Increasing the barrier by 0.4 kcal/mol yields $nT_1 = 1.6$ s and NOE = 2.8 for vinyl-2, in reasonable agreement with experiment. However, the values of $nT_1 = 3.6$ s and NOE = 2.9 for vinyl-1, although improved, remain in poor agreement with experiment. The apparent too-fast rate of rotation for the vinyl side group, even after increasing the rotational energy barriers, may be a consequence of the small size of the $C(sp^2)H_2$ group as represented in the united atom force field. The correlation times for the C−H vectors are about a factor of 2 longer for the modified force field compared to the original force field, reflecting the increased rotational energy barriers. It can be seen that for the nuclei with NOE values significantly reduced from 3, i.e., the trans sp^2 nuclei and the backbone nuclei near the vinyl side group, the long-time tail makes a significant contribution to the C−H $P_2(t)$, indicating an important contribution of nonlocal motions to the decay of the magnetization for these nuclei. Note that in agreement with experiment, the T_1 values for the trans sp^2 nuclei are quite similar to those for the cis sp^2 nuclei despite the quite different NOE values, indicating that local motions occur at about the same rate.

The torsional autocorrelation functions for the various bonds are shown in Figure 4. In addition to the cis and trans allyl dihedrals and the β dihedrals, we also show the autocorrelation functions for the vinyl and α dihedrals (see Figure 3 for labeling). The dihedral autocorrelation times for the allyl trans and the β dihedrals for the modified force field are approximately twice as long as those for the original force field, again reflecting increased rotational energy barriers. For the allyl cis dihedral, a smaller difference is seen, probably as a result of efforts to minimize differences in populations for the modified potential. The vinyl dihedral (without increased rotational barrier) shows behavior qualitatively similar to that for the allyl cis dihedral. The α dihedrals, i.e., the backbone bonds neighboring the vinyl side group, exhibit behavior qualitatively similar to that of the much slower β dihedrals. Because the T_1 and NOE values for the branch (v_B) and α carbon nuclei are accurately reproduced (see Table 2), we conclude that the simulations accurately reproduce the rate of conformational dynamics for the α dihedrals. Therefore, we conclude that one important impact of vinyl groups on the local dynamics is an increase in the β-like character of the backbone; each vinyl group contributes two slow β-like dihedrals to the backbone and no fast allyl dihedrals.

Chain Dynamics. From $\tilde{S}(q, t)$ a self-diffusion coefficient $D_R = 3.4 \times 10^{-7}$ cm^2/s is obtained (eq 10), in much better agreement with the value determined from NSE measurements than what was obtained in the original simulations. From the chain center of mass displacement (eq 16), a value of 3.2×10^{-7} cm^2/s is obtained. These values are 20−30% greater than D_{NSE} obtained from NSE measurements. In our united atom polyethylene simulations, a center of mass self-diffusion coefficient 40−45% larger than experiment was obtained for n-$C_{44}H_{90}$,[2] whereas the value was approximately 30% larger than experiment for n-$C_{100}H_{202}$.[4] A comparison of $S(q, t)$ from the modified potential with experiment as a function of scaled time is shown in Figure 5. Agreement with experiment is somewhat improved at shorter times for the larger q values and is similar in quality to that obtained for PE.[4] The end-to-end vector autocorrelation function, illustrated in Figure 6, yields a Rouse time of $\tau_R = 16$ ns through application of eq 18, whereas application of eq 11 yields $\tau_R = 15$ ns. These values are in good agreement with the value of $\tau_R = 17-21$ ns obtained from applying eq 11 to the experimental data.

VI. Conclusions

In this work, we have performed a detailed comparison between simulations and experiment of the local and chain dynamics of a melt of 1,4-polybutadiene. Quantitative reproduction of the experimental results required a careful matching of the relevant average experimental chain length and architecture in the simulated model. Our quantum chemistry-based force field reproduces the measured melt density reasonably well. Chain conformations, as determined through the radius of gyration, are in excellent agreement with the experimental results. Using a united atom representation of the quantum chemically determined conformational energetics, however, resulted in a too-fast rate of conformational transitions as demonstrated through a comparison of spin lattice relaxation times, as determined from NMR, with those determined from simulation. In the case of PBD, we can resolve 12 different local environments in the chain and therefore have detailed information about the local torsional dynamics. We found similar behavior in an earlier comparative study of an all-atom and a united atom representation of alkane chains. To compensate for this shortcoming of the united atom representation, we increased the torsional barriers by 0.4 kcal/mol, after which we were able to reproduce all but one vinyl spin lattice relaxation time to within 20%.

The chain dynamics in the melt were measured via neutron spin−echo experiments for a range of length scales covering the internal random-walk structure of the chains. Determining the center of mass diffusion coefficient from the scattering curves at small momentum transfers, we again observe a discrepancy of about 30% between experiment and simulation, consistent with the accuracy with which the local dynamics are reproduced in the simulation. The small angle scattering can be reasonably described with the Rouse model

prediction. At larger momentum transfers, however, the Rouse model prediction systematically deviates from the experimental as well as from the simulated scattering curves. It had been argued that this deviation is due to the neglect of local stiffness effects in the Rouse model.[15] Using the prediction of a semiflexible chain model and the contour length and persistence length as they can be determined from the simulation, however, showed that our chains are so flexible that there is only a small difference between the Rouse prediction and the prediction from the semiflexible chain model. Both show the same deviation from the observed scattering. One can match the observed scattering curves with the prediction from the semiflexible chain model by artificially increasing the chain stiffness, but the parameters are then in strong disagreement with the observed chain structure determined from simulation.

To conclude, we can say that we have validated our improved force field for 1,4-polybutadiene through careful comparison with NMR and NSE experiments on the local and chain dynamics of this polymer in the melt. From this starting point, we will now look at the temperature dependence of the dynamics in this glass-forming polymer with the long-term aim of gleaning mechanistic information on the molecular motions giving rise to the different relaxation processes at lower temperatures.

Acknowledgment. G.D.S. gratefully acknowledges support provide by the American Chemical Society, Petroleum Research Fund through Grant 98-13330, and SFB262 for support for his stay in Mainz. This research was funded in part by the University of Utah Center for the Simulation of Accidental Fires and Explosions (C-SAFE), funded by the Department of Energy, Lawrence Livermore National Laboratory, under Subcontract B341493.

References and Notes

(1) Smith, G. D.; Yoon, D. Y.; Zhu, W.; Ediger, M. D. *Macromolecules* **1994**, *27*, 5563.
(2) Paul, W.; Yoon, D. Y.; Smith, G. D. *J. Chem. Phys.* **1995**, *103*, 1702.
(3) Smith, G. D.; Paul, W.; Yoon, D. Y.; Zirkel, A.; Hendricks, J.; Richter, D.; Schober, H. *J. Chem. Phys.* **1997**, *107*, 4751.
(4) Paul, W., Smith, G. D.; Yoon, D. Y.; Farago, B.; Rathgeber, S.; Zirkel, A.; Willner, L.; Richter, D. *Phys. Rev. Lett.* **1998**, *80*, 2346.
(5) Paul, W.; Smith, G. D.; Yoon, D. Y. *Macromolecules* **1997**, *30*, 7772.
(6) Smith, G. D.; Yoon, D. Y.; Wade, C. G.; O'Leary, D.; Chen, A.; Jaffe, R. L. *J. Chem. Phys.* **1997**, *96*, 3798.
(7) Johari, G. P.; Goldstein, M. *J. Chem. Phys.* **1970**, *53*, 2372.
(8) Smith, G. D.; Paul, W. *J. Phys. Chem. A* **1998**, *102*, 1200. For the branch carbon and vinyl carbons, the nonbonded potential for an sp^2 carbon was employed. It was necessary to include a hydrogen atom at each branch (chiral) carbon. The hydrogen atoms interact with neighboring carbon atoms through C−C−H bending potentials with a force constant of 86 kcal/rad^2 and a tetrahedral equilibrium angle. The hydrogen atoms have no nonbonded interactions with other atoms.
(9) Baschnagel, J.; Paul, W.; Tries, V.; Binder, K. *Macromolecules* **1998**, *31*, 3856.
(10) Gisser, D. J.; Glowinkowski, S.; Ediger, M. D. *Macromolecules* **1991**, *24*, 4270.
(11) Moe, N. E.; Ediger, M. D. *Macromolecules* **1996**, *29*, 5484.
(12) Dejean de la Batie, B.; Laupretre, F.; Monnerie, L. *Macromolecules* **1989**, *22*, 122.
(13) Monkenbusch, M.; Schaetzler, R.; Richter, D. *Nucl. Inst. Methods* **1997**, *A399*, 301.
(14) Rouse, P. E. *J. Chem. Phys.* **1953**, *21*, 1272; Doi, M.; Edwards, S. F. *The Theory of Polymer Dynamics* Clarendon Press: Oxford, 1989.
(15) Harnau, L.; Winkler, R.; Reineker, P. *J. Chem. Phys.* **1997**, *106*, 2460.
(16) Flory, P. J. *Statistical Mechanics of Chain Molecules*; Hanser: New York, 1969.
(17) Reinhardt, L.; Fytas, G.; Fischer, E. W.; Willner, L. *Acta Polym.* **1996**, *47*, 399.
(18) Frisch, M. J.; Trucks, G. W.; Schlegel, H. B.; Scuseria, G. E.; Robb, M. A.; Cheeseman, J. R.; Zakrzewski, V. G.; Montgomery, J. A., Jr.; Stratmann, R. E.; Burant, J. C.; Dapprich, S.; Millam, J. M.; Daniels, A. D.; Kudin, K. N.; Strain, M. C.; Farkas, O.; Tomasi, J.; Barone, V.; Cossi, M.; Cammi, R.; Mennucci, B.; Pomelli, C.; Adamo, C.; Clifford, S.; Ochterski, J.; Petersson, G. A.; Ayala, J. Y.; Cui, Q.; Morokuma, K.; Malick, D. K.; Rabuck, A. D.; Raghavachari, K.; Foresman, J. B.; Cioslowski, J.; Ortiz, J. V.; Stefanov, B. B.; Liu, G.; Liashenko, A.; Piskorz, P.; Komaromi, I.; Gomperts, R.; Martin, R. L.; Fox, D. J.; Keith, T.; Al-Laham, M. A.; Peng, C. Y.; Nanayakkara, A.; Gonzalez, C.; Challacombe, M.; Gill, P. M. W.; Johnson, B.; Chen, A.; Wong, M. W.; Andres, J. L.; Gonzalez, C.; Head-Gordon, M.; Replogle, E. S.; Pople, J. A. *Gaussian 98*, rev. A.1; Gaussian, Inc.: Pittsburgh, PA, 1998.
(19) Tuckerman, M. E.; Tobias, D. J.; Klein, M. L.; Martyna, G. *Mol. Phys.* **1996**, 87, 1117.

MA991130Z